PHYSICAL REVIEW C VOLUME 18, NUMBER 2 AUGUST 1978

Classical, semiclassical, and quantum mechanical calculations for scattering and reactions of $^{16}O + ^{208}Pb$*

Louis C. Vaz
Department of Chemistry, State University of New York at Stony Brook, Stony Brook, New York 11794 and Departmento de Fisica Nuclear, I.F. U.F.R.J., Cidade Universitaria, Ilha do Fundao, Rio de Janeiro, R. J. Brasil 20.000

John M. Alexander
Department of Chemistry, State University of New York at Stony Brook, Stony Brook, New York 11794

E. H. Auerbach
Department of Physics, Brookhaven National Laboratory, Upton, New York 11973
(Received 1 November 1977)

Correspondences are shown between semiclassical and quantum mechanical calculations that employ the same real potential. Comparisons are made to experimental scattering, complete fusion, and total reaction cross sections for $^{16}O + ^{208}Pb$. The separate roles of rainbow and absorptive effects are shown. Deductions of the nuclear potential from fits to data clearly depend on the adopted sequence of data fitting procedures and the freedom given at each stage to the parameters of the chosen potential. It is this sequence that plays a large role in the inference of weak vs intermediate vs strong surface absorption. The sequence we choose implies intermediate surface absorption for this case. Parameter adjustments are explored for data fits that employ the proximity potential.

[NUCLEAR REACTIONS Classical, semiclassical, and quantum mechanical analysis for the system $^{16}O + ^{208}Pb$. Elastic scattering, fusing, and all reactive collisions are treated and related to classical turning points for each l wave.]

I. INTRODUCTION

A widely used approach to reaction phenomena begins with the parametrization of a real two-body one-dimensional potential-energy function and separately a device or devices to describe reaction (or absorption) probabilities of various sorts.[1] For interactions between complex nuclei, the real and imaginary parts of a phenomenological optical potential are often employed in quantum mechanical[2] and/or semiclassical[3] calculations. Classical mechanics is also, of course, used to advantage with a real potential and some auxiliary assumption(s) to specify reaction probabilities.[4] The quantum mechanical optical-model codes[5] have few mathematical approximations but require many parameters whose roles are interwoven and thus hard to separate. By contrast classical and semiclassical calculations usually involve more approximations but can often be characterized by parameters whose meaning is more transparent than the quantum mechanical ones.[6] This transparency can be very useful for building intuition and identifying the relationship between various measurements and the parameters in the model potentials.[3,6]

It is well known that experimental data for one type (e.g., elastic scattering or reaction cross sections of a given class) can be accounted for by very different potential-energy functions. Even the basically different effects of absorption and refraction are not easily separated by comparisons of theoretical calculations to experimental results. Most comparisons have focused on one class of experimental data to the near exclusion of other sources. In this study we successively modify a nuclear potential to attempt to account for three kinds of experimental data, cross sections for elastic scattering, fusing collisions, and all reactions. We start with an empirically developed real potential based on total reaction cross sections and quarter-point angles for elastic scattering. We try to develop a feeling for the different roles of the real and imaginary potentials by the comparison of classical approach distances and deflection angles to quantum mechanical transmission coefficients. By iterative modifications of the potential we achieve reasonable fits to the data, but we stop short of using energy dependent potentials.

For this exercise we use the same real potentials (an empirical one or the proximity potential[7]), and we calculate transmission coefficients either by pure quantum mechanics via the code ABACUS-3 or via an empirical formula obtained from data systematics.[8] Second, we use the extensive experimental studies of Videbaek *et al.*[9] and others[10] to estimate the radial extent of the absorption for the system $^{16}O + ^{208}Pb$. For elastic scattering we note separately the rainbow and absorptive effects on the gross cutoff from Rutherford scattering and

also on the more detailed shape of the elastic angular distributions. And finally, we discuss comparisons to calculations involving the proximity potential which is proving to be very useful for the description of interactions between complex nuclei.[11]

II. OBJECTIVES AND METHODS OF CALCULATIONS

A. Roadmap

The first objective of this study is to develop a feeling for the relationship between classical trajectory calculations and quantum mechanical, optical-model calculations. We use a particular real potential (Fig. 1) to calculate classical deflection angles and approach distances (Fig. 2). Then with the same real potential in the optical model (ABACUS-3),[5] along with a Woods-Saxon imaginary potential of varying radius parameter r_I, we obtain values of transmission coefficients $(T_l), l_{1/2}$ (the particular l with $T_l = \frac{1}{2}$), reaction and elastic cross sections (σ_R and σ_{el}) for each input value of r_I. We show the dependence of $l_{1/2}$ and $\theta_{1/4}$ (quarter-point angle for elastic scattering) on r_I (Figs. 3 and 4). From the classical trajectories we obtain strong absorption distances $D_{1/2}$ (approach distance for $l_{1/2}$) and compare them to the classical rainbow distances R_r (Fig. 2).

These various relationships between the classical and quantum mechanical parameters give a picture of scattering and reaction patterns from the limit of rainbow dominance to that for surface absorption.

We then associate the complete fusion cross section σ_{cf} with the reaction cross section in an optical model with absorption confined to the interior. In this model the dependence of σ_{cf} on energy (at low energies) can be used to fix the s-wave barrier in the real potential (or the fusion barrier). Similarly in the limit of weak surface absorption the value of $\theta_{1/4}$ depends on the real potential near the rainbow distance (Figs. 2, 4–6). If strong absorption occurs outside R_r (i.e., $D_{1/2} > R_r$) then the value of $\theta_{1/4}$ depends on the imaginary potential (Figs. 2–4). In addition, the difference between σ_R and σ_{cf} as a function of incident energy gives a reflection of the extension of the absorptive potential beyond the maximum in the real potential (Fig. 7).

For the reactions of ^{16}O with ^{208}Pb we make a series of comparisons to experimental data.[9] We find that for energies greater than ≈90 MeV refractive (or rainbow) scattering seems to dominate. In this picture the strong absorption distance $D_{1/2}$ remains almost constant with energy while the fusion distance R_m varies with energy. This suggests the possible applicability of several simple semiclassical parametrizations for measured

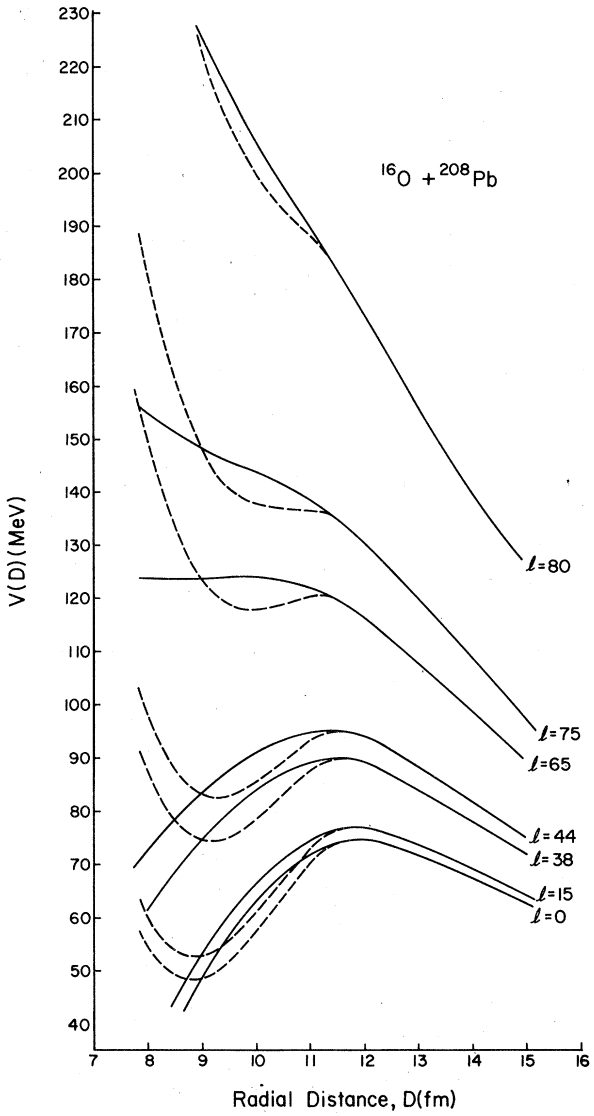

FIG. 1. The l-dependent real potential from Eqs. (13) and (14), with $V_N(R_0) = 4.0$ MeV, $\hbar\omega_0 = 4$ MeV, $R_0 = 12$ fm, and $E_0 = 74.77$ MeV. This potential is compared to the real potential, proximity [(Eqs. (17)–(24)]. ($b = 1$ F, $\Delta R = +0.28$ fm, $\Delta\gamma = -0.0317$ MeV fm^{-2}) plus Coulomb potentials [Eqs. (25)–(27)]. The s-wave potentials are compared in detail in Table I.

quantities: (1) To estimate σ_R one might use the Hill-Wheeler formula with the approximation of a constant mean absorption radius.[12] (2) For σ_{cf} one might also use the Hill-Wheeler formula, but with a fusion radius R_m that decreases with increasing energy.[13] (3) For $\theta_{1/4}$ ($E > 90$ MeV) one might use semiclassical formulas for rainbow scattering.[14-16] These treatments are briefly touched here and explored further in the following paper.[14]

Finally, we use the proximity potential[7] for some similar calculations and comparisons. Certain

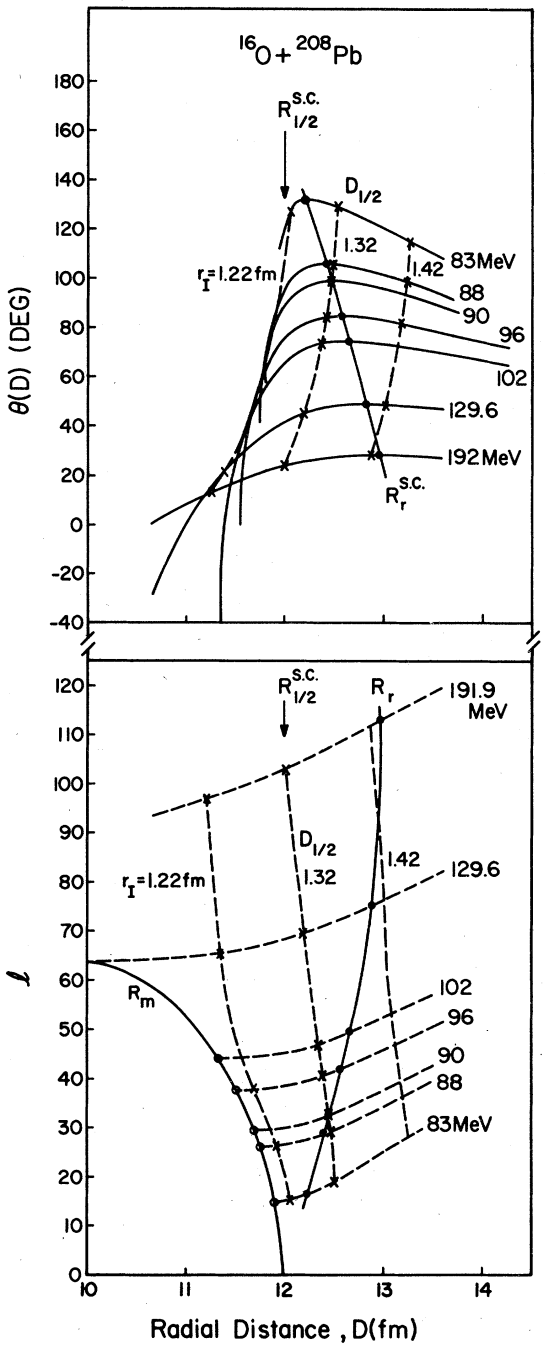

FIG. 2 (a) The classical deflection functions at several angles versus distance of closest approach. R_r is the rainbow distance. The distance $R^{sc}_{1/2} = 12$ fm corresponds to $l_{1/2}$ in the empirical semiclassical systematics of Ref. 8. The $D_{1/2}$ values correspond to $l_{1/2}$ values calculated with ABACUS-3, for imaginary Woods-Saxon potentials with $W_0 = 10$ MeV, $a_I = 0.5$ fm, and r_I as indicated and the empirical real potential given in Fig. 1 and Table I. (b) Classical values of l vs distance of closest approach. Also shown are the orbiting l, rainbow l, and values of $l_{1/2}$ for various values of r_I.

kinds of parameter modifications are shown to be necessary to obtain fits to experimental data.

B. Methodology

The methods of classical, semiclassical, and quantum mechanical calculations have been developed by many workers over a long period. The particular equations and assumptions that we use are fully described elsewhere[5,8,14] so we will only give a brief outline of the major inputs. Quantum mechanical calculations have been performed with the code ABACUS-3, described in Ref. 5. It rests on an optical potential with real (or refractive) and imaginary (or absorptive) parts. For the imaginary potential we used the conventional Woods-Saxon form

$$W(r) = -iW_0/\{1 + \exp[(r - R_I)/a_I]\}, \tag{1}$$

where W_0, R_I, and a_I are the depth, radius, and diffuseness of the imaginary well. We have made a series of calculations that employ the same real potential in classical, semiclassical, and quantum mechanical machinery. This exercise was to obtain the correspondences between the semiclassical and quantum mechanical formalisms. The classical deflection angle $\theta(l$ or $b)$ and the distance of closest approach D for each impact parameter b are obtained as follows:

$$\theta(l) = \pi - 2\int_D^\infty (b/r^2)[1 - (b/r)^2 - V(r)/E]^{-1/2} dr\,, \tag{2}$$

where

$$1 - (b/D)^2 - V(D)/E = 0, \tag{3}$$

and $V(D)$ is the sum of nuclear plus Coulomb potentials.

Cross sections for complete fusion are calculated with the often made assumption of friction free passage over or through the real barrier.[13,17] In the optical model this situation was simulated by using a complex potential of small radius ($r_I = 1.12$ fm). Our semiclassical approximation to this situation is to calculate the transmission coefficients from the Hill and Wheeler formula[18]

$$T_l(E) = \{1 + \exp[(2\pi/\hbar\omega_m)(E_{lm} - E)]\}^{-1}, \tag{4}$$

where

$$E_{lm} = V_c(R_m) + V_n(R_m) + (l + \tfrac{1}{2})^2\hbar^2/2\mu R_m^2, \tag{5}$$

and

$$\hbar\omega_m = \left|(\hbar^2/\mu)d^2V(r,l)/dr^2\right|_{R_m,\, l_{crit}}^{1/2}. \tag{6}$$

R_m and l_{crit} are obtained from Eqs. (7) and (8),

$$dV(r,l)/dr\,\big|_{R_m,\, l_{crit}} = 0, \tag{7}$$

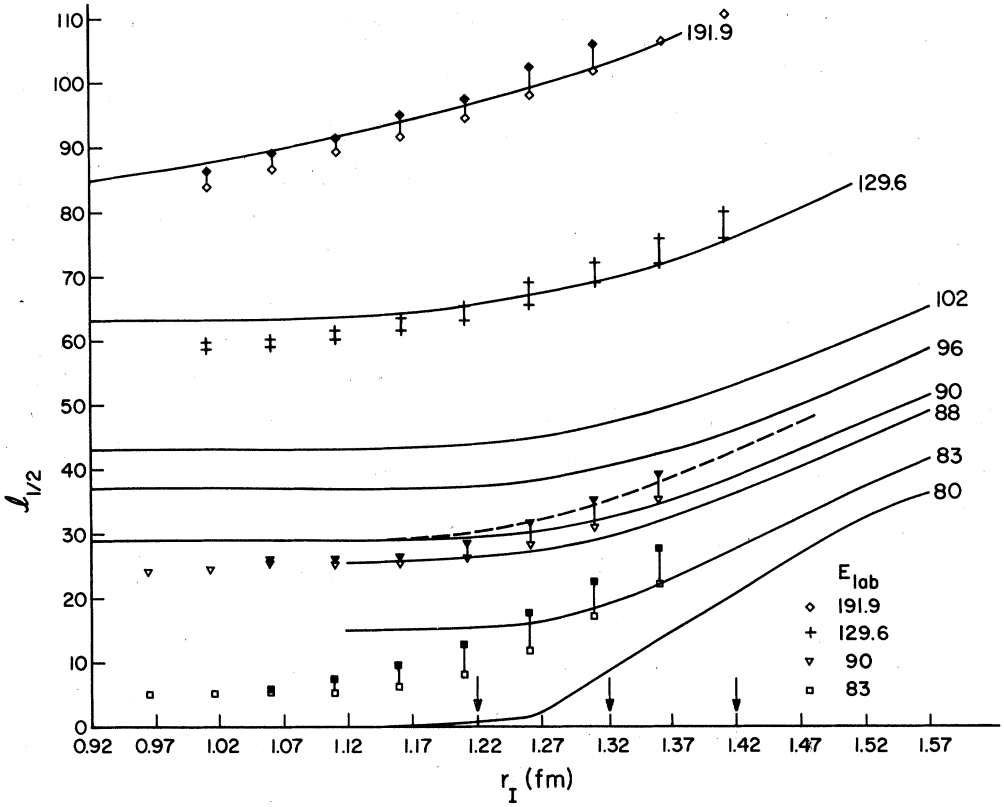

FIG. 3. ABACUS-3 calculations of $l_{1/2}$ vs r_I for $W_0 = 10$ MeV and $a_I = 0.5$ fm. One curve is shown for $W_0 = 20$ Mev and $a_I = 0.5$ fm. For those cases shown by smooth curves the empirical real potential was used (Fig. 1 and Table I). For the points a parametrization was taken from Ref. 10 (lower points $a_I = 0.45$, upper points $a_I = 0.60$ see the Appendix).

$$E = V(r,l)_{R_m, l_{\rm crit}} = V_c(R_m) + V_n(R_m) + (l_{\rm crit} + \tfrac{1}{2})^2\hbar^2/2\mu R_m^2, \quad \text{for } E < E_{lm}^{\max}, \tag{8}$$

where

$$l_{\rm crit} = (R_m/\lambda\!\!\!^{-})[1 - V(R_m)/E]^{1/2}. \tag{9}$$

R_m is the location of the maximum in $V(r,l)$, and $E_{lm}^{\max}$ is the energy where the maximum in $V(r,l)$ just disappears. These transmission coefficients [Eq. (4)] in turn specify the fusion cross section

$$\sigma_{\rm cf} = \pi\lambda\!\!\!^{-2}\sum_{l=0}^{\infty}(2l+1)T_l(E). \tag{10}$$

Note that R_m decreases with increasing energy [in contrast to Eq. (28) later].

For the reactions of ^{16}O with ^{208}Pb, the optical-model calculations show that the strong absorption distance is almost independent of energy. This observation suggests the possible applicability of the Wong treatment for the total reaction cross sections.[8,12] Here one also uses Hill-Wheeler transmission coefficients but with the values of E_l given in terms of the height E_0' and radius R_0' of the s-wave barrier $[E_0' = V_c(R_0') + V_N(R_0')]$

$$E_l = V_c(R_0') + V_N(R_0') + (l+\tfrac{1}{2})^2\hbar^2/(2\mu R_0'^2), \tag{11}$$

with curvative $\hbar\omega_0$. In this approximation the mean absorption radius R_0' is assumed to be independent of l and E, and the parameters need not necessarily be related to the real potential maximum.

For incident energies greater than 90 MeV for ^{16}O + ^{208}Pb, the rainbow distance seems to be greater than the mean absorption distance. This suggests that the rainbow effect may be responsible for the gross cutoff of the elastic scattering from the Rutherford values. Thus a semiclassical formulation of rainbow scattering may suffice to describe this cutoff. In this approximation[14-16] the essentially classical cross sections $\sigma_i(l)$ are obtained for each branch i of the deflection function from the relation

$$\sigma_i(l) = \lambda\!\!\!^{-2}(l+\tfrac{1}{2})[\sin\theta\,|d\theta(l)/dl|]^{-1}[1 - T_l(E)], \tag{12}$$

with absorption included via transmission coefficients from Eq. (4) with E_l given by Eq. (11) and $\hbar\omega_0 = 4$ MeV. These elastic cross sections for each trajectory are then summed via the uniform approximation to allow for interferences for angles less than the rainbow angle θ_r.[14,15] For angles

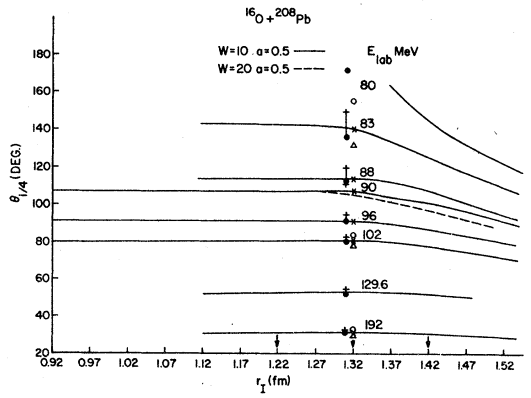

FIG. 4. Calculated values from ABACUS-3, are shown for $\theta_{1/4}$ vs r_I for various incident energies: solid lines from the empirical potential of Fig. 1; ⊙ with empirical potential $E_0=75.77$ MeV, $R_0=11.99$ fm, and $\hbar\omega_0=4.0$ MeV; Δ with empirical potential $E_0=73.77$ MeV, $R_0=11.99$ fm, and $\hbar\omega_0=4.0$ MeV. In all cases (except for the symbol +) $W_0=10$ MeV, $a_I=0.5$ fm, and $r_I=1.32$ fm. Experimental values from Ref. 9 are shown as X. For the symbol (Ref. 5) + and ⊙ a parametrization was taken from Ref. 10 (see the Appendix): $+a_I=0.45$ fm; ⊙ $a_I=0.60$ fm.

larger than the rainbow angle the spreading of the wave packets is approximated by an equation due to Da Silveira.[16]

For most calculations that are presented here we use an empirical potential[8,14]

$$V(r)=E_0-[(\hbar\omega_0)^2/(2\hbar^2/\mu)](r-R_0)^2, \quad \text{for } r\leq R_0, \tag{13}$$

and

$$V(r)=V_c(r)+V_N(r) = V_c(r)+V_N(R_0)\exp[-(r-R_0)/d], \quad \text{for } r\geq R_0, \tag{14}$$

with

$$V_c(r)=Z_PZ_Te^2/r, \quad \text{for } r\geq R_0. \tag{15}$$

The continuity of $V(r)$ at R_0 requires that d be given by

$$d=-R_0V_N(R_0)/V_c(R_0). \tag{16}$$

If the s-wave interaction barrier E_0 is found empirically to be equal to the s-wave fusion barrier E_{0m}, then one would expect one radius (R_0) to be appropriate to both.[17] If $E_{0m}>E_0$ then different radii are expected for interaction and for fusion and some adjustments are required in Eqs. (11), (13), (14). For reaction systems with $Z_PZ_T\leq 1000$ these empirical barriers seem to be very close indeed.[8,19]

We also explore briefly the proximity potential[7]

$$V_P(\xi)=4\pi\gamma\bar{R}b\Phi(\xi). \tag{17}$$

The proximity potential function $\Phi(\xi)$ is given by

$$\Phi(\xi\leq 1.2511)=-\tfrac{1}{2}(\xi-2.54)^2-0.0852(\xi-2.54)^3, \tag{18}$$

$$\Phi(\xi\geq 1.2511)=-3.437\exp(-\xi/0.75), \tag{19}$$

where

$$\xi\equiv s/b, \quad s=r-C_T-C_P, \tag{20}$$

and b is surface width.

The surface energy coefficient γ is given by

$$\gamma=0.9517[1-1.7826(N-Z)^2/A^2]+\Delta\gamma, \tag{21}$$

and N, Z and, A refer to the combined system of the two interacting nuclei. The radius $\bar{R}$ is given by

$$\bar{R}=C_TC_P/(C_T+C_P), \tag{22}$$

where C is the nuclear central density radius calculated for the effective sharp radius R from the formulas

$$R=1.28A^{1/3}-0.76+0.8A^{-1/3}+\Delta R \tag{23}$$

and

$$C=R(1-b^2/R^2). \tag{24}$$

The surface energy coefficient [Eq. (21)] and the radii R from Eq. (23) were varied from those originally proposed[7] by the arbitrary addition of $\Delta\gamma$ and ΔR chosen to reproduce the experimental fusion cross sections. For the Coulomb potential we used

$$V_c(r)=Z_PZ_Te^2/r, \quad \text{for } r>R_c \tag{25}$$

and

$$V_c(r)=(Z_PZ_Te^2/2R_c)(3-r^2/R_c^2), \quad \text{for } r<R_c, \tag{26}$$

where

$$R_c=1.30(A_P^{1/3}+A_T^{1/3}). \tag{27}$$

These two nuclear potentials for $^{16}O+^{208}Pb$ are compared in Table I for $l=0$. Also, the l-dependent empirical potential is shown with the associated l dependence of R_m in Fig. 1.

III. COMPARISONS BETWEEN CLASSICAL, SEMICLASSICAL, AND QUANTUM MECHANICAL CALCULATIONS

As mentioned in the previous section most calculations we will show were made with the empirical real potential given in Table I and Fig. 1 [Eqs.

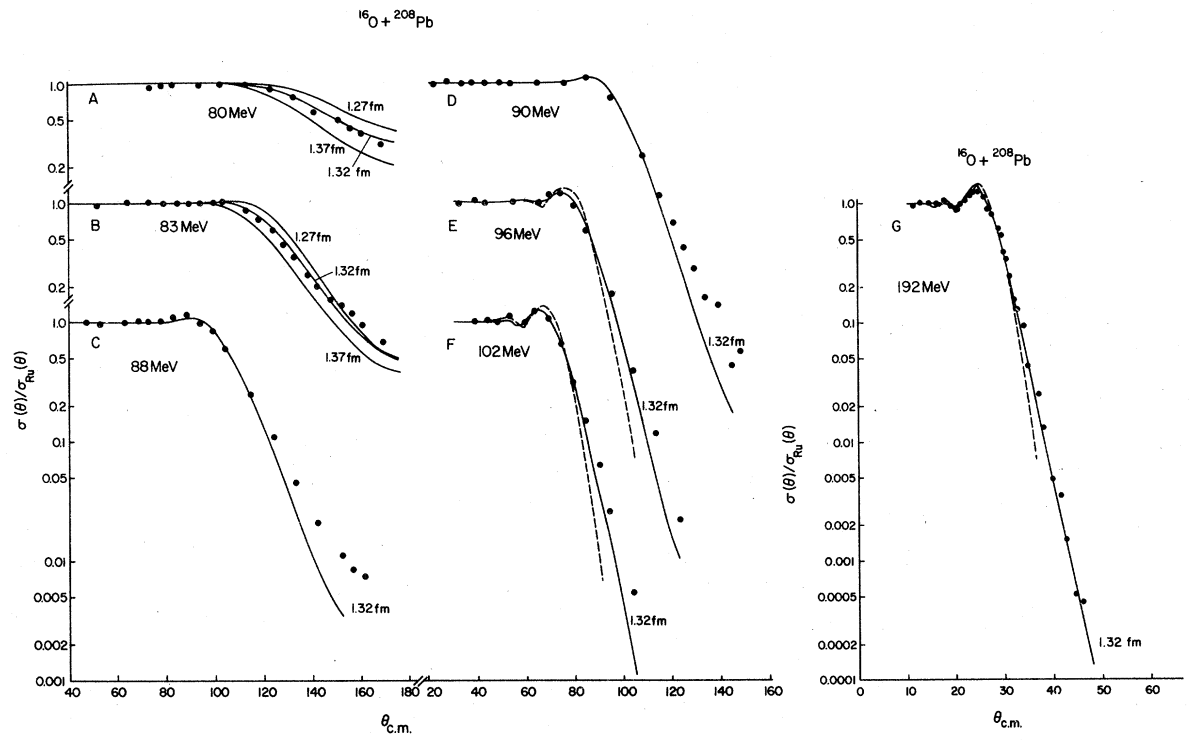

FIG. 5. (a)–(g) Elastic scattering solid lines represent results calculated with ABACUS-3 for various values of r_I and dashed lines represent the semiclassical calculation of Ref. 14. The empirical potential was the same used in Fig. 1. Data points are from Refs. 9 and 10.

(13)–(16)] with $V_N(R_0) = -4.0$ MeV, $\hbar\omega_0 = 4$ MeV, $R_0 = 12$ fm, and $E_0 = 74.77$ MeV. This empirical potential has a shape similar to the more fundamental proximity potential which we explore in more detail later. The first step in classical and semiclassical calculations is the determination of the deflection function $\theta(l)$. Also of great pictorial value is the distance of closest approach $D(l)$. The relationships between these three quantities (classical deflection angle θ, incident angular momentum $l\hbar$, and classical distance of closest approach, D) are shown in Figs. 2(a) and 2(b).

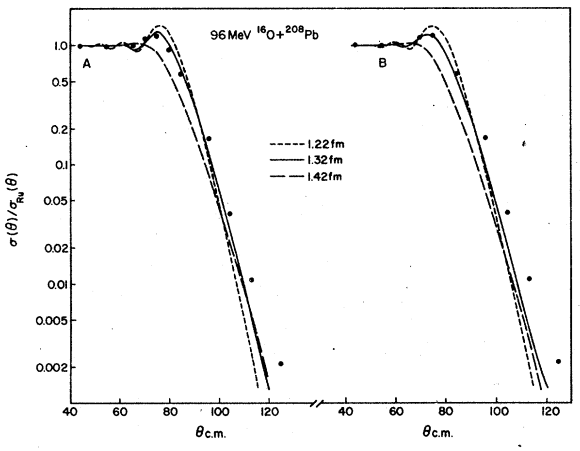

FIG. 6. Elastic scattering calculations with ABACUS-3 and several values of r_I: (a) for empirical real potential (shown in Fig. 1), (b) for proximity potential ($b = 1$ fm, $\Delta R = +0.28$ fm, $\Delta\gamma = -0.0317$ MeV fm^{-2}). In each case $W_0 = 10$ MeV and $a_I = 0.5$ fm.

Figures 1 and 2 carry a lot of information that can help to extend our feeling for the various features of scattering and reaction cross sections. The relationships between classical D and θ and the mean absorption l are quite revealing. The orbiting distances R_m for each partial wave l are shown for energies below 129 MeV, and the very significant energy variation of the radius for orbiting R_m is apparent in both figures. For this potential, orbiting disappears for $E > 130$ MeV. In Fig. 2(a) we see a rainbow angle (maximum in θ) for all energies, even those well above that for the disappearance of the orbiting condition. The rainbow distance R_r increases with increasing incident energy. That distance $D_{1/2}$ corresponding to the transmission coefficient $T_l = \frac{1}{2}$ (calculated by ABACUS-3) is also shown for three different imaginary potentials and for an earlier empirical correlation.[8] It is interesting that the strong absorption distances $D_{1/2}$ as well as the orbiting distance

TABLE I. Comparison of proximity and empirical nuclear potentials (MeV).

Radial distance (fm)	$b=1$ fm $\Delta R=0$ fm $\Delta\gamma=0$ (MeV/fm^2)	Proximity $b=1$ fm $\Delta R=+0.280$ $\Delta\gamma=-0.0317$ (MeV/fm^2)	$b=0.85$ fm $\Delta R=+0.358$ $\Delta\gamma=-0.0354$ (MeV/fm^2)	$b=0.81$ fm $\Delta R=+0.429$ $\Delta\gamma=-0.0400$ (MeV/fm^2)		Empirical[a]
10.04	21.185	34.907	36.230	38.595	(37.502)[b]	30.149
10.64	10.569	22.583	23.734	26.478	(26.550)	19.207
11.04	6.200	14.691	15.241	17.675	(17.524)	13.369
11.64	2.786	6.612	6.058	7.018	(7.176)	6.734
12.04	1.634	3.879	3.235	3.633	(3.515)	3.697
12.64	0.734	1.743	1.262	1.353	(1.111)	1.383
13.04	0.431	1.022	0.674	0.701	(0.504)	0.718
13.64	0.194	0.459	0.263	0.261	(0.152)	0.269
14.04	0.114	0.270	0.141	0.135	(0.068)	0.140

[a] Calculated with $E_0=74.77$ MeV; $\hbar\omega_0=4.0$ MeV; $V_N(R_0)=-4.0$ MeV and $R_0=11.99$ fm.
[b] Woods-Saxon potential obtained by least squares fit to this modified proximity potential is enclosed in parentheses: $V_0=-45.504$ MeV; $r_0=1.279$ fm; $a=0.497$ fm.

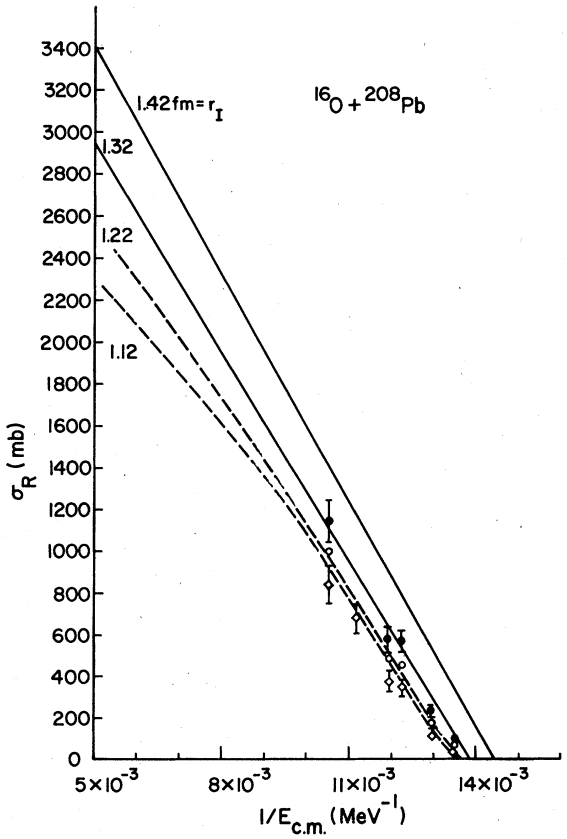

FIG. 7. Cross sections for fusion, ◇; total reaction, ⊙; and reaction less inelastic ^{16}O, O vs E^{-1}. Curves were calculated by ABACUS-3, with the real empirical potential in Table I, W_0 = 10 MeV, a_I = 0.5 fm and various r_I as indicated. Data from Ref. 9.

R_m all decrease with increasing energy, in contrast to the increase shown for the rainbow distance R_r. In Fig. 2 we see that the strong absorption distance is greater than the rainbow radius ($D_{1/2}>R_r$) for $r_I=1.42$ fm. Thus strong surface absorption will dominate both scattering and reaction cross sections if nature favors this case. On the contrary, if nature favors the case of imaginary radius $r_I=1.22$ fm (or the empirical $R_{1/2}=12$ fm) then $R_r>D_{1/2}$ and the rainbow phenomenon will often dominate the gross cutoff of elastic scattering. Intermediate behavior would result from the situation shown for $r_I=1.32$ fm.

For the quantum mechanical calculations with the same empirical real potential (and $W_0=10$ MeV, $a_I=0.5$ fm) the values of $l_{1/2}$ are shown vs r_I in Fig. 3. (Consider here only the smooth curves in Fig. 3; we return to the points in the Appendix.) For energies less than 130 MeV we note that $l_{1/2}$ is essentially independent of absorptive potential for $r_I\leq 1.12$ fm, but that $l_{1/2}$ increases with r_I or W_0 for $r_I>1.12$ fm. This corresponds to the screening role of the real potential for energies below 130 MeV; only the lower l waves surmount the barrier in Fig. 1 and enter the absorptive region (for $r_I\leq 1.12$ fm). For energies below 130 MeV we will relate the behavior corresponding to $r_I<1.12$ fm to the measured fusion cross sections. The strong dependence of $l_{1/2}$ on r_I for high energy (>130 MeV) and large r_I simply reflects the increased radial extent of $W(r)$ compared to $V(r)$. For the higher energies we see no obvious intuitive connection between r_I and the fusion phenomenon. (The three arrows simply provide reference points between various figures.) The fuzzy edge of the reaction probability ($l_{T_I=0.9}-l_{T_I=0.1}$) is significantly greater for all these imaginary potentials than for the empirical treatment of Ref. 8 [Eqs. (10) and

(11)].

The quarter-point angle $\theta_{1/4}$ (that angle where the elastic scattering σ_{el} is $\frac{1}{4}$ the Rutherford value) is commonly used to characterize the gross cutoff of elastic scattering. In Fig. 4 we show values of $\theta_{1/4}$ as calculated by ABACUS-3, for various imaginary potentials and the empirical real potential used for Figs. 1–3. (Consider here only the smooth curves in Fig. 4 and the points at $r_I = 1.32$ fm: We return to the points at $r_I = 1.31$ fm in the Appendix.) The important role of $W(r)$ is clear for energies near the barrier (where $D_{1/2} > R_r$, see Fig. 2) as well as its decreasing role for higher energies (where $R_r > D_{1/2}$). By contrast the sensitivity of $\theta_{1/4}$ to the real potential is shown at all energies by the points at $r_I = 1.32$ fm. These reflect the steep deflection functions at low energies that gradually flatten with increasing energy as shown in Fig. 2(a). One, therefore, expects the real potential to dictate the value of $\theta_{1/4}$ for elastic scattering at 130 and 192 MeV, but absorption could be very important for near barrier energies depending on its exact radial extent. For intermediate energies (88–102 MeV) either could rule.

In Figs. 5(a)–5(g) and 6 we look at the elastic scattering distributions in more detail. It is apparent at 80 MeV that absorption is very important at angles greater than 120° ($D_{1/2} > R_r$ in Fig. 2). Here we are below the real barrier, and the tail of $W(r)$ extends beyond the maximum in $V(r)$ where it nips a few of the projectiles as they pass. At higher energies (see Fig. 6 for example) absorption controls all the important angles if $r_I > 1.42$ fm as was indicated in Figs. 2–4. For $r_I = 1.32$ fm or less, however, $V(r)$ sets $\theta_{1/4}$ by the rainbow effect while $W(r)$ governs the size of the peak σ_{el}/σ_{Ru} and the slope for $\theta > \theta_{1/4}$. This point, as shown in Fig. 6, has been often emphasized by others.[10] Figures 5(e)-5(g) show that the semiclassically calculated elastic cross sections [Eqs. (13)–(21) of Ref. 14] give essentially the same values of $\theta_{1/4}$ but differ in the peak cross sections and in the slope of σ_{el} vs θ. These differences are due to a combination of the different forms of T_l vs l and possibly to some of the semiclassical approximations.

In Fig. 7 we show reaction cross sections as calculated by ABACUS-3 with imaginary potentials having different radii. The plot is made versus $E_{c.m.}^{-1}$ as is often done for analysis of data[1] via the classical equation

$$\sigma_R = \pi R_{slope}^2 (1 - E_{int}/E) = \pi R_{slope}^2 - (\pi R_{slope}^2 E_{int}) E^{-1}. \quad (28)$$

It is interesting to analyze these calculated curves in the conventional way. The curves for $r_I = 1.42$ and 1.32 fm are indeed linear, and the others have a nearly linear region for $9 \times 10^{-3} < E^{-1} < 13 \times 10^{-3}$. In Table II the values of R_{slope} and E_{int} from Fig. 7 are compared to the corresponding values of $D_{1/2}$ from Fig. 2 and $V(D_{1/2})$ from Eq. (14). The values of the approach distance vary somewhat with energy so the comparison is not completely unambiguous. Nevertheless, we can conclude that the values of R_{slope} are within ≈0.3 fm of the values of $D_{1/2}$ at high energy and the corresponding values of E_{int} are within 1.7 MeV of $V(D_{1/2})$ at near barrier energies.

If it is reasonable to associate the fusion cross sections with an imaginary well of small radius (e.g., $r_I = 1.12$ fm), then the classical analysis should give a good estimate of the real potential maximum. The linear portion of the plot used to evaluate R_{slope} for this case should be in the energy range $(E_{lm}^{max})^{-1} < E^{-1} \lesssim (1.05 E_{0m})^{-1}$. Similarly the analysis of reaction cross sections should give a decent estimate of the mean absorption radius $D_{1/2}$ and a slight underestimate of the associated real potential $V(D_{1/2})$. A comparison of fusion and reaction cross sections can reflect the extent of absorptive processes at distances outside the real potential maximum.

It seems clear that we must obtain an initial orientation concerning the relative importance of refraction versus absorption for each case of interest. This orientation is of crucial importance to the sequence of fitting steps and therefore to the number of parameters left free for each successive fit to experiment. If the common intuitive picture of fusing collisions is correct, then a consideration of the fusion cross section at each bombarding energy can lead to the energy of the corresponding real potential maximum. Then a consideration of the total reaction cross section can give a reasonably good idea of the relation between R_m and $D_{1/2}$, and $\theta_{1/4}$ can fix the real potential at the strong absorption radius or the rainbow radius,

TABLE II. Apparent radii and barriers compared with respective input quantities.

r_I (fm)	R_{slope} [a] (fm)	E_{int} [a] (MeV)	$D_{1/2}$ [b] (fm)	$V(D_{1/2\,max})$ [c] (MeV)	Δ [d] (MeV)
1.12	≈11.7	74.3	−12.0	74.7	0.4
1.22	≈11.7	73.5	11.6 − 12.2	74.6	1.1
1.32	12.1	72.4	12.0 − 12.5	73.8	1.4
1.42	12.9	69.3	12.9 − 13.2	71.0	1.7

[a] Empirically evaluated by fitting $\sigma_R = \pi R_{slope}^2 (1 - E_{int}/E)$ to the values of σ_R calculated by ABACUS-3 and in Fig. 7.

[b] Closest approach distance in Fig. 2 corresponding to $l_{1/2}$ calculated by ABACUS-3.

[c] Coulomb plus nuclear potential evaluated at the maximum $D_{1/2}$ in Fig. 2.

[d] $\Delta = V(D_{1/2\,max}) - E_{int}$.

whichever is larger. This interplay can suggest whether $D_{1/2} > R_r$ or $R_r > D_{1/2}$. Finally, more detailed fits can be made to elastic scattering data with the imaginary potential shape left free but with the real potential constrained to maintain an adequate description of σ_R, σ_{cf}, and $\theta_{1/4}$. In the next section we follow this sequence for $^{16}O + ^{208}Pb$; in the Appendix we discuss some comparisons to the potential from Ref. 10.

IV. COMPARISONS TO EXPERIMENTAL RESULTS

In Table III, we give the measured cross sections for fusion (column 5), all reactions (last column), and all reactions except inelastically scattered ^{16}O (column 8). As mentioned in connection with Fig. 3, we might identify complete fusion ($E < 130$ MeV) with the reaction cross section obtained from ABACUS-3 with an absorptive potential of $r_I = 1.12$ fm (column 4). Columns 2 and 3 give semiclassically calculated fusion cross sections obtained as described in Sec. II, [column 2 from the empirical potential of Eqs. (13)–(16), column 3 from an adjusted proximity potential]. In each case the calculated values are slightly greater than the measured ones (by about 2–33%). This reflects a real barrier height E_{0m} that is slightly too low (≈ 0.7 MeV) and/or too fat. This comparison is also shown in Fig. 7, where the cross sections are plotted against E^{-1} as is often done for data analysis.[19] The curves are those calculated via ABACUS-3 with the empirical potential [$E_0 = 74.77$ MeV, $\hbar\omega_0 = 4.0$ MeV, $R_0 = 11.99$ fm, and $V_N(R_0) = -4$ MeV] and various imaginary potential radii as indicated.

The measured reaction cross sections (column 12, Table III) are consistent with absorption characterized by $r_I = 1.32$ fm (column 10, Table III). The strong absorption case for $r_I = 1.42$ fm (column 9, Table III) gives reaction cross sections that are much too large. The empirical semiclassically calculated reaction cross sections (column 6 in Table III) are compared to the reaction cross section excluding inelastic ^{16}O. The empirical systematics leading to these values would have usually excluded inelastic scattering and so we also exclude it for this comparison.[8,14] ABACUS-3 calculations with an absorptive potential having $r_I = 1.22$ fm (column 7, Table III) give about the same behavior as this empirical formula.

From these comparisons we conclude that the intermediate surface absorption case characterized by $r_I = 1.32$ fm gives a best fit for the true total reaction cross section; the weaker surface absorption of $r_I = 1.22$ fm describes all those reactions except inelastic scattering and the no-surface-absorption of $r_I < 1.12$ fm describes the

TABLE III. Calculated and experimental values of fusion and reaction cross sections (mb).

	Complete fusion				Reaction (less inelastic ^{16}O)				Total reaction			
E_{lab} (MeV)	σ_{cf} [a] Empirical potential	σ_{cf} [b] Proximity potential	σ_Q [c] ABACUS-3 $r_I = 1.12$	σ_{exp} [d] Fusion	σ [e] Empirical semiclassical	σ_Q [c] ABACUS-3 $r_I = 1.22$	σ_{exp} [d] Reaction except ^{16}O	σ_Q [c] ABACUS-3 $r_I = 1.42$	σ_Q [c] ABACUS-3 $r_I = 1.32$	σ_Q [f] (Ref. 10)	σ_{exp} [d] All reactions
80		19		36 ± 4	15	43	64	334	127	227	100 ± 10
83	144	136	144	108 ± 10	136	169	177	510	272	381	237 ± 21
88	390	373	385	350 ± 40	383	414	455	786	530	645	572 ± 41
90	478	460	473	377 ± 50	475	504	486	888	625	744	578 ± 56
96	717	696	710	685 ± 70	729	749		1168	887	1013	
102	921	901	913	844 ± 90	952	962	1000	1413	1115	1248	1157 ± 94
129.6	1540	1568	1543		1710	1656		2235	1877	2036	
192		1389	2172			2415		3180	2742	2938	

[a] Calculated with the sharp cutoff equation, $\sigma_{cf}(E) = \pi\lambda^2(l_{crit}+1)^2$ with l_{crit} obtained from Eq. (9) and the empirical potential [Eq. (13)] with $E_0 = 74.71$ MeV, $R_0 = 11.90$ fm, and $\hbar\omega_0 = 4.5$ MeV.

[b] Calculated as in (a) but with the proximity potential with $b = 1$ fm and $\Delta R = +0.28$ fm, $\Delta\gamma = -0.0317$ MeV/fm^2 (Table I, column 3).

[c] Calculated with ABACUS-3 using empirical potential $E_0 = 74.77$ MeV, $R_0 = 11.99$ fm, $\hbar\omega_0 = 4$ MeV and $V_N(R_0) = -4$ MeV, $W_0 = 10$ MeV, $a_I = 0.5$ fm and r_I as indicated (in fm).

[d] From Ref. 9, fission cross sections have been identified here as fusion.

[e] Calculated as in Ref. 8 with Eqs. (10) and (11) and the same real potential as in footnote c.

[f] Calculated with ABACUS-3 with Woods-Saxon potentials from Ref. 10; $V = 43$ MeV, $r_V = 1.20$ fm, $a_V = 0.70$ fm, $W = 15$ MeV, $r_I = 1.31$ fm, $a_I = 0.60$ fm.

complete fusion cross sections (for $E < 130$ MeV).

In Figs. 5, the best fit to elastic scattering by ABACUS-3 is also provided by an absorptive potential with a radius parameter of 1.32 fm. The semiclassical calculations in Ref. 14 give reasonable values of $\theta_{1/4}$ but only low-quality fits to the elastic scattering near the maximum in σ_{el}/σ_{Ru} or for $\theta > \theta_{1/4}$. As shown previously in Figs. 4 and 5, the fit to σ_{el}/σ_{Ru} near $\theta_{1/4}$ is quite sensitive to the real potential (for $E > 83$ MeV or $r_I < 1.32$ fm) while the absorptive potential is quite important for other angular regions. For the near-barrier energies 80 and 83 MeV in Figs. 5(a) and 5(b), respectively, the absorptive effects are important for all angles, and $r_I = 1.32$ fm gives the best fit.

In Fig. 8, we compare the "sensitive radii" R_s reported by Videbaek *et al.*[9] to the rainbow radii R_r from Fig. 2. The very interesting decrease at low energies runs counter to one's intuitive feeling that elastic scattering probes smaller radial distances at higher energies. Indeed the mean absorption radii do decrease with increasing energy as shown in Fig. 2, but we infer from the parallel behavior of R_r and R_s that radial distances near that for the rainbow ray are most important in the quantum mechanical fitting from Ref. 9. Also shown in Fig. 8, are ratios of imaginary to real potentials evaluated at R_r and R_s. These values are ≈ 0.3 compared to ≈ 0.8 obtained by Ball *et al.*[10] from elastic scattering fits with more parameter freedom. One's deductions of the nuclear potential seem to depend on the order of his fitting procedure and the relative weight given to each data type. Our procedure emphasizes σ_{cf}, σ_R, and σ_{el}; Ball *et al.*[10] emphasize σ_{el} alone, and in particular they require a good fit to the peak values of σ_{el}/σ_{Ru}. The importance of real versus imaginary potentials is clearly a delicate one. We infer that for this case $R_r > D_{1/2}$ for $E \geq 88$ MeV and thus that a primary adjustment should be the value of $V(R_r)$ to achieve a fit to $\theta_{1/4}$. Then the imaginary potential should be adjusted to try to fit the shape of the elastic scattering (σ_{el} vs θ).

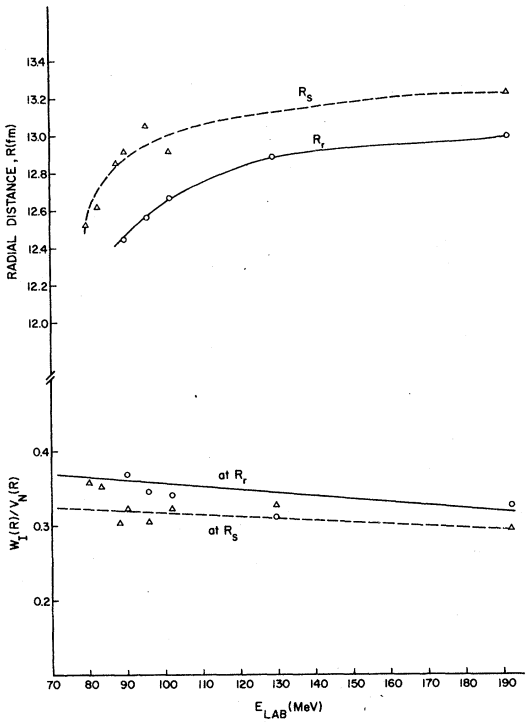

FIG. 8. Rainbow radius R_r and the "sensitive radius", R_s (reported in Ref. 9) versus incident energy. Also shown are the ratios of imaginary ($W_0 = 10$ MeV, $a_I = 0.5$ fm, $r_I = 1.32$ fm) to the real empirical (shown in Fig. 1) potentials at R_r and R_s. Lines are drawn only to guide the eye. For comparison $W(R_r)/V(R_r)$ is ≈ 0.08 and ≈ 0.014, for $r_I = 1.22$ and 1.12 fm, respectively.

Our feeling is that the sequence just employed provides a reasonable order of parameter refinement for this case, namely: (a) Adjust the real potential maximum to be consistent with complete fusion cross sections (for energies less than 130 MeV); (b) adjust the shape of the real potential near R_r to be consistent with the values of σ_{el} near the quarter point $\theta_{1/4}$; (c) adjust the gross features of the absorptive potential to be consistent with total reaction cross sections; (d) refine the shape of the absorptive potential to improve the quality of the fits to elastic scattering for $\theta > \theta_{1/4}$ and near the peaks in σ_{el}/σ_{Ru}. In the next section we report some initial steps toward this end with the proximity potential.

V. PARAMETER ADJUSTMENTS FOR THE PROXIMITY POTENTIAL TO FIT FUSION, REACTION AND, ELASTIC SCATTERING CROSS SECTIONS

As described in the literature for years and in the sections above and in the Appendix we can see that it is indeed difficult to obtain a perfect fit to all kinds of data with a two-body potential independent of energy. However, if one adopts functional forms for the real and imaginary potentials one may systematically adjust the parameters until some kind of compromise fit is attained. Such systematic fits have often begun with elastic scattering data. We choose to begin with fusion cross sections and $\theta_{1/4}$ values as we feel that these quantities focus on the real potential at its maximum and near the rainbow radius, respectively. Then we move to the reaction cross section and the shape of the elastic scattering to begin to refine the imaginary potential.

We use here the proximity and Coulomb potentials [Eqs. (17)–(27)] for the real potential and the Woods-Saxon form for the imaginary potential [Eq. (1)]. There are three parameters in the proximity potential R, b, and γ, each of which the authors[7] feel is already reasonably well limited by the physical content of the model. However, each of these can be considered to have some adjustability[7] without violation of the spirit of the original model. In the last section we made an adjustment in R and γ [$\Delta R = +0.280$ fm, Eq. (23), $\Delta\gamma = -0.0317$ MeV fm^{-2}, Eq. (21)] to alter the barrier height and position and thus improve the description of the fusion cross sections. In Table I, columns 2 and 3, we show the original and the modified forms, respectively, and in Table III, we compare the measured fusion cross sections to the calculated ones [obtained with the modified potential (column 3, Table III)]. This modification makes a significant change in the potential (see Table I) and is necessary to fit σ_{cf}.[20] (This problem is discussed further in the Appendix for the potential of Ref. 10.)

The second step in our potential refinement is to improve the fit to $\theta_{1/4}$. This quantity depends mainly on the real potential near R_γ or at ≈12.7 fm (Fig. 8). In Table I, column 3 we see that the modified proximity potential is ≈0.4 MeV more attractive than the empirical potential at 12.7 fm and its calculated value of $\theta_{1/4}$ is correspondingly smaller, ≈2° at 96 MeV, for example. Adjustment of the imaginary potential could not cure this problem (Fig. 6). Thus we resort to adjustment of b, R, and γ in the potential while constraining the resulting E_{0m} to retain the fit to σ_{cf}. Two such potentials explored as examples are (a) $b = 0.85$ fm, $\Delta R = +0.358$ fm, $\Delta\gamma = -0.0354$ MeV fm^{-2} and (b) $b = 0.81$ fm, $\Delta R = +0.429$ fm, $\Delta\gamma = -0.0400$ MeV fm^{-2}.[21]

As we turn to the energy dependence of the elastic scattering, each of these potentials can give rather good fits for some energies. However, both of them give systematic deviations at some energies if W, a_I, and r_I are not allowed an energy dependence. Potential (a) overestimates σ_{el} at 80 and 83 MeV and to a lesser extent from 88–102 MeV. Potential (b) does a better job at lower energies by systematically underestimates σ_{el} for $\theta > \theta_{1/4}$ at higher energies.

These details of the elastic scattering are sensitive to all the fine points of both the real and imaginary potentials: (1) functional forms, (2) energy dependences, (3) small deviations from the frozen shape idealization, etc. Therefore, we have not attempted a further improvement of the fit. We simply conclude that it is possible to achieve a good description of σ_{cf} and $\theta_{1/4}$ with a modified proximity potential. Also, one can obtain an associated imaginary potential and fit σ_R and many but not all features of the elastic scattering. These real and imaginary potentials have intermediate to weak surface absorption with both rainbow and absorptive effects on the elastic scattering.

VI. SUMMARY

The procedure that we have used begins with a trial real potential which has a maximum at ≈12.0 fm. The variations of this potential have not deviated greatly in this respect. The value of the real potential at the maximum has been adjusted to fit measured fusion cross sections. The quarter-point angle for elastic scattering has been used to constrain the real potential between 12.4 and 12.8 fm (see R_γ in Figs. 2 and 8). The relationship between fusion and reaction cross sections has been used as an indicator of the strong absorption radius 12.0–12.4 fm ($D_{1/2}$ for $r_I = 1.32$ fm in Fig. 2). The shape of the elastic scattering patterns has also been used to reflect the combined effects of real and imaginary potentials. The elastic scattering fits are good for 80, 83, and 192 MeV but poor for $\sigma/\sigma_{Ru} \leq 0.1$ for $88 < E < 102$ MeV. The use of an energy dependent potential has not been explored.

It is, of course, possible that one could achieve comparable or even better data fits with other potentials. The fusion cross sections are quite sensitive to the height of the potential barrier but not very sensitive to its radial extent. A weaker real potential would still require a real maximum of ≈75 MeV but could have R_{0m} smaller than 12 fm. Nevertheless, the quarter-point angles would require a nuclear potential of ≈1.4 MeV at ≈12.6 fm. Likewise the reaction cross sections require a somewhat lower barrier than 75 MeV at a strong absorption radius ≈0.5–1 fm greater than that for the real potential maximum. As many of the nonfusing reactions lead to inelastic scattering, the complete interpretive pattern depends on an appropriate treatment of these very soft collisions. The compilation of values of $\theta_{1/4}$ in Refs. 22–24 is probably perturbed by the inclusion of inelastic scattering along with the elastic. The compilation of σ_R values in Ref. 8 probably excludes inelastic scattering in almost all cases. These aspects are discussed in the following paper.[14]

We are grateful to R. Satchler for helpful comments on the Appendix.

APPENDIX

In Ref. 10 Ball *et al.* made a careful study of a

number of potentials as they relate to elastic scattering by ^{208}Pb. For the case of ^{16}O they fitted several potentials to the elastic scattering data at 192 and 129.5 MeV. They found that very good fits required somewhat different parametrization at each energy, but they did not explore the question of energy-dependent potentials in much detail. We wish to put their work in the context of this study and for this purpose we use a set of Woods-Saxon parameters they presented as a compromise set [$V = 43$ MeV, $r_v = 1.20$ fm, $a_v = 0.70$ fm, $W = 15$ MeV, $a_I = 0.60$ fm (and 0.45 fm), and $r_I = 1.31$ fm]. For the discussion of elastic scattering and total reaction cross sections we focus on $r_I = 1.31$ fm; for the discussion of fusion we vary r_I as discussed before for Fig. 3.

From the discussion of Tables II–IV and Figs. 3 and 7 we can anticipate that the Ball parameters will underpredict σ_{cf}. Their values of R_0 and E_0 are 11.5 fm and ≈77 MeV. A good fit in Table IV requires an E_0 value of ≈75 MeV. The strong effect of this difference is evident from the comparisons for $l_{1/2}$ shown in Fig. 3 and for σ_{cf} as given in Table IV.

It is very interesting that the values of σ_R and $l_{1/2}$ from the potential of Ref. 10 for $r_I = 1.31$ and $a_I = 0.60$ fm are significantly different from those from the other potentials (see Fig. 3 and Table III). However, if one changes the value of a_I only slightly to 0.45 fm the reaction cross sections are improved (Fig. 3). Evidently the choices of $V(r)$ and $W(r)$ can essentially compensate as far as they predict the reaction cross section. However, this is not the case if in addition one considers the elastic scattering as can be seen for the values of $\theta_{1/4}$ in Fig. 4. The parameter set from Ball *et al.* with $a_I = 0.45$ gives increasingly larger values of $\theta_{1/4}$ with decreasing energy. The set with $a_I = 0.60$ fits well for $E > 90$ MeV but for < 90 MeV gives values of $\theta_{1/4}$ that are too small. Their best fit at 129.5 MeV did require a stronger real potential than at 192 MeV. This trend is consistent with the systematic deviation pattern we show in Fig. 4.

We conclude that a parametrization which starts by fits to elastic scattering at high energies will not necessarily fit the scattering of low energies. Also such a parametrization should not be expected to be a good predictor of fusion cross sections at low energies. Here, of course, we assume that the generally used model of complete fusion is applicable. Namely, we assign to fusion those impacts that lead to friction free traversal of the real potential maximum ($E \leq E_{lm}^{max}$). Furthermore, we identify such traversals in quantum mechanics with the plateau in Fig. 3. Another model of the fusion process could, of course, lead to different results and conclusions. For example, as pointed out by Birkelund and Huizenga,[25] frictional energy loss could occur before the collision partners arrive at the radius corresponding to the real potential maximum. If this situation obtains then the empirical fusion barrier will demand an even stronger real potential than we or others[4,17,19] have heretofore adopted. In turn this would call for weaker absorptive potentials in the surface in order to main-

TABLE IV. Calculated and experimental cross sections for fusion σ_{cf} (mb) and all reactions σ_R (mb).

E_{lab} (MeV)	σ_{exp} [a] All reactions	σ_Q [b] ABACUS-3 $r_I = 1.30$	σ_Q [c] ABACUS-3 $r_I = 1.30$	σ_{exp} [a] Fusion	σ_{cf} [d]	σ_{cf} [e]	σ_{cf} [f]	σ_Q [g] Abacus-3 $r_I = 1.02$	σ_Q [h]
80	100 ± 10	98	107	36 ± 4	10	11	21	18	
83	237 ± 21	230	249	108 ± 10	99	104	134	117	37
88	572 ± 41	482	504	350 ± 40	331	341	376	354	250
90	578 ± 56	577	599	377 ± 50	417	430	466	442	333
96		835	858	685 ± 70	652	671	711	681	555
102	1157 ± 94	1061	1085	844 ± 90	855	881	924	889	737

[a] Experimental data from Ref. 9.

[b] Calculated with ABACUS-3 with the proximity potential ($b = 0.85$ fm, $\Delta R = +0.358$ fm, $\Delta\gamma = -0.0354$ MeV fm^{-2} and $W_0 = 10$ MeV, $r_I = 1.30$ fm, and $a_I = 0.499$ fm). $E_{0m} = 75.36$ MeV, $R_{0m} = 11.89$ fm.

[c] Calculated with ABACUS-3 with proximity potential ($b = 0.81$ fm, $\Delta R = +0.429$ fm, $\Delta\gamma = -0.040$ MeV fm^{-2} and $W_0 = 10$ MeV, $r_I = 1.30$ fm and $a_I = 0.50$ fm). $E_{0m} = 74.84$ MeV, $R_{0m} = 11.99$ fm.

[d] Calculated with Eqs. (4)–(10) with the proximity potential ($b = 1.0$ fm, $\Delta R = +0.238$ fm, $\Delta\gamma = -0.028$ MeV fm^{-2}). $E_{0m} = 75.39$ MeV, $R_{0m} = 11.69$ fm.

[e] Calculated with Eqs. (4)–(10) with real potential of footnote b.

[f] Calculated with Eqs. (4)–(10) with real potential of footnote c.

[g] Calculated with ABACUS-3 with the proximity potential of footnote b and $W_0 = 10$ MeV, $r_I = 1.02$ fm, $a_I = 0.499$ fm.

[h] Calculated with ABACUS-3 with Woods-Saxon real potential from Ref. 10, footnote f Table III.

tain the fit to $\theta_{1/4}$ from the elastic scattering (see Fig. 4).

Note added in proof. Calculations based on a one-body friction model have just been published.[26] The results for $E \leq E_{lm}^{max}$ are very similar to those from Sec. IIB Eqs. (4)–(10).

---

*Supported in part by FINEP and CNPq of Brazil and by U. S. Energy Research and Development Administration and U. S. Department of Energy Contract No. EY-76-C-02-0016.

[1]A. Fleury and J. M. Alexander, Annu. Rev. Nucl. Sci. 24, 279 (1974), and references therein.

[2]P. E. Hodgson, Annu. Rev. Nucl. Sci. 17, 1 (1967); D. M. Brink, J. Phys. 37, C5-47 (1976).

[3]R. A. Broglia and A. Winther, Phys. Rep. 4C, 153 (1972); N. Glendening, in *Proceedings of the International Conference on Reactions Between Complex Nuclei, Nashville, 1974*, edited by R. L. Robinson, F. K. McGowan, J. B. Ball, and J. H. Hamilton (North-Holland, Amsterdam, 1974) p. 38; J. Knoll and R. Schaeffer, Ann. Phys. (N.Y.) 97, 307 (1976).

[4]R. Bass, Phys. Lett. B47, 139 (1973); Nucl. Phys. A231, 45 (1974); Phys. Rev. Lett. 39, 265 (1977).

[5]E. H. Auerbach, Code A-THREE (ABACUS-3) BNL Report No. 23001, 1977 (unpublished). E. H. Auerbach and C. E. Porter, in *Proceedings of the Third Conference on Reactions Between Complex Nuclei*, edited by A. Ghiorso, R. Diamond, and H. Conzett (Univ. of California Press, 1963).

[6]P. R. Christensen and A. Winther, Phys. Lett. 65B, 19 (1976).

[7]J. Blocki, J. Randrup, W. J. Swiatecki, and C. F. Tsang, Ann. Phys. (N.Y.) 105, 427 (1977).

[8]L. C. Vaz and J. M. Alexander, Phys. Rev. C 10, 464 (1974); J. M. Alexander, L. C. Vaz, and S. Y. Lin, Phys. Rev. Lett. 33, 1487 (1974).

[9]F. Videbaek, R. B. Goldstein, L. Grodzins, S. G. Steadman, T. A. Belote, and J. D. Garrett, Phys. Rev. C 15, 954 (1977).

[10]J. B. Ball, C. B. Fulmer, E. E. Gross, M. L. Halbert, D. C. Hensley, C. A. Landemann, M. J. Saltmarsh, and G. R. Satchler, Nucl. Phys. A252, 208 (1975).

[11]See, for instance, W. U. Schroder and J. R. Huizenga, Annu. Rev. Nucl. Sci. 27, 465 (1977).

[12]C. Y. Wong, Phys. Lett. 42B, 186 (1972); Phys. Rev. Lett. 31, 766 (1973).

[13]W. J. Swiatecki, Lawrence Berkeley Laboratory, Report No. 4296, 1975 (unpublished).

[14]L. C. Vaz and J. M. Alexander, following paper, Phys. Rev. C 18, 833 (1978).

[15]M. V. Berry and K. E. Mount, Rep. Prog. Phys. 35, 315 (1972).

[16]R. DaSilveira, in *Proceedings of the International Conference on Reaction Between Complex Nuclei, Nashville, 1974*, edited by R. L. Robinson, F. K. McGowan, J. B. Ball, and J. H. Hamilton (North-Holland Amsterdam, 1974).

[17]D. Glas and U. Mosel, Phys. Rev. C 10, 2620 (1974); Nucl. Phys. A237, 429 (1975).

[18]D. L. Hill and J. A. Wheeler, Phys. Rev. 89, 1102 (1953).

[19]W. Scobel, H. H. Gutbrod, M. Blann, and A. Mignerey, Phys. Rev. C 14, 1808 (1976); H. H. Gutbrod, W. G. Winn, and M. Blann, Nucl. Phys. A213, 267 (1973).

[20]L. C. Vaz and J. M. Alexander. Results of analysis of the available experimental data to date indicate that the *a priori* proximity potential of Ref. 7 predict fusion barriers that are too high and an underestimate of complete fusion cross section. Results to be published.

[21]Both retain good fits to total reactions (Table IV, columns 3 and 4). Both also fit σ_R values with $W_0 = 10$ MeV, $r_I = 1.30$ fm, and $a_I = 0.50$ fm. However, for $E \geq 83$ MeV while potential (a) retains a good fit to σ_{cf} (Table IV, column 7), potential (b) (Table IV, Column 8) slightly overestimates the measured σ_{cf} by 4–20%.

[22]J. M. Alexander, H. Delagrange, and A. Fleury, Phys. Rev. C 12, 149 (1975).

[23]J. R. Birkelund, J. R. Huizenga, H. Freiesleben, K. L. Wolf, J. P. Unik, and V. E. Viola, Phys. Rev. C 13, 133 (1976).

[24]W. Scobel, J. Bisplinghoff, M. Blann, A. Mignerey, P. David, J. Ernst, and T. Mayer-Kuckuh, Z. Phys. A284, 343 (1978).

[25]J. R. Birkelund and J. R. Huizenga, Phys. Rev. C 17, 126 (1978).

[26]J. R. Birkelund, J. R. Huizenga, J. N. De, and D. Sperber, Phys. Rev. Lett. 40, 1123 (1978).